Composites Part C: Open Access 18 (2025) 100633

Contents lists available at ScienceDirect

Composites Part C: Open Access

journal homepage: www.elsevier.com/locate/composites-part-c-open-access

Influence of the position of fibre misalignment in glass fibre-reinforced polymers on mechanical properties, damage behaviour and traceability via non-destructive tests

Jonas Drummer [a,*], Tim Luplow [b], Linus Littner [c], Richard Protz [d], Sebastian Heimbs [b], Marc Kreutzbruck [c], Maik Gude [d], Bodo Fiedler [a]

[a] Hamburg University of Technology, Institute of Polymers and Composites (IPC), Denickestraße 15, 21073 Hamburg, Germany
[b] Technische Universität Braunschweig, Institute of Aircraft Design and Lightweight Structures (IFL), Hermann-Blenk Straße 35, 38108 Braunschweig, Germany
[c] University of Stuttgart, Institut für Kunststofftechnik (IKT), Pfaffenwaldring 32, 70569 Stuttgart, Germany
[d] TUD Dresden University of Technology, Institute of Lightweight Engineering and Polymer Technology (ILK), Holbeinstraße 3, 01307 Dresden, Germany

ARTICLE INFO

Keywords:
Manufacturing defects
Stress concentration
Progressive failure
Component design
Safety factor

ABSTRACT

Defects in glass fibre-reinforced polymers (GFRP), especially fibre misalignments, are a well-known issue affecting structural performance. This paper investigates how the position of such misalignments influences the mechanical behaviour to deepen the understanding of their influence. GFRP cross-ply laminates with 11 fibre layers were fabricated using the resin transfer moulding process, containing four different types of fibre misalignments. Subsequently, the specimens were evaluated by computed tomography scans and ultrasonic testing and experimentally investigated under tensile, compressive, and bending loading. The obtained mechanical properties were also compared with simulation data. The results of the mechanical tests show that the strength reduction varies greatly depending on the load case, the type of misalignment and its position. Undulations in tensile tests can lead to a strength reduction as low as 8 %, while a single fold located outside the middle layer can reduce the compressive strength by up to 37 %. In service life tests, the effect is even more pronounced. In the worst case, the presence of multiple defects can reduce the service life by up to 94 %. The simulation results showed that a local displacement of individual layers does not represent the extent of undulations and that existing simulation approaches need to be revised and extended. The results of the experiments and simulations demonstrate that both the presence and the position of fibre misalignments significantly affect the material behaviour and are likely underestimated in current research.

1. Introduction

As a result of their excellent specific mechanical properties and corrosion resistance, fibre-reinforced polymers (FRP) are a widely used construction material. In recent years, more and more fibre-reinforced composite parts are used in heavy-duty applications [1–4]. As a consequence of high loads, the size and wall thickness of FRPs are generally increasing, resulting in thicknesses of up to 100 mm for wind turbine blades [5]. Due to the statistically distributed number of defects, thicker composite parts often display more defects in total compared to smaller parts. Similarly, increasing size also leads to manufacturing deviations. This can lead to residual stresses resulting in fibre misalignments [6–8] or other defects, such as voids, dry spots, etc. [9–13]. These defects are commonly known to result in stress concentrations and ultimately lead to a reduction in mechanical properties [14–18]. Because it is nearly impossible to create defect-free structures economically, it is important to understand how these defects affect the failure behaviour of composites. To analyse and better understand their effects on mechanical properties, it is necessary to introduce reproducible defects in composite parts and systematically investigate their impact [19].

Although numerous studies have investigated the influence of defects on the mechanical properties of FRPs for individual load cases, the effect of the position of such defects on the overall laminate behaviour has received comparatively little attention so far. Fibre misalignment is one of the most common manufacturing defects and can be classified into in-plane undulations, misalignments within a ply, and out-of-plane undulations, misalignments in the thickness direction of the laminate [20]. In thick laminates, these defects typically occur randomly, so that misalignments near the surface are just as likely

* Corresponding author.
E-mail address: jonas.drummer@tuhh.de (J. Drummer).

https://doi.org/10.1016/j.jcomc.2025.100633
Received 8 May 2025; Received in revised form 30 July 2025; Accepted 31 July 2025
Available online 8 August 2025

as those in the mid-plane. It is known from previous studies that induced delaminations tend to become more critical the closer they are located to the outer surfaces of a laminate [21]. Furthermore, fibre misalignments and other local defects often act as initiation sites for delamination [22,23]. Based on this knowledge, the present study aims to investigate not only whether fibre misalignments affect the overall mechanical behaviour of the composite, but also to what extent their position through the laminate thickness influences the material response.

For this study, glass fibre-reinforced polymers (GFRPs) that contain typical types of in-plane or out-of-plane fibre misalignments were produced. The specimens were then evaluated by X-ray computed tomography scans (CT) as well as ultrasonic testing and experimentally investigated under tensile, compressive, and bending loading at room temperature. Finally, these results were compared with simulation results to check how well standard simulation programmes can estimate the effects of fibre misalignments.

2. Materials and methods

2.1. Manufacturing of GFRP plates and test specimens with defined fibre misalignment

The investigated GFRP was manufactured using the resin transfer moulding process. The matrix material is Loctite MAX 2 (Henkel Adhesives, Germany), a widely used high-performance polyurethane system with a tensile stiffness of 2.9 GPa, a tensile strength of 84.3 MPa, and a glass transition temperature (T_g), defined via DMA as the maximum of the loss modulus E'', of approximately 115 °C [24]. The fibre reinforcement is a woven 2 × 2 twill glass fibre fabric 05507-FK144 (Valmiera Glass, Latvia) with an areal weight of 280 g/m^2 and a warp tensile strength of 300 N/cm [25]. After laying the fibre layers by hand, the infusion and curing process was carried out according to the manufacturer's recommendation: one hour at 80 °C and an additional hour of post-curing at 150 °C. Differential scanning calorimetry (DSC) confirmed that the resin system reached full cure under these processing conditions.

Independent of the type of experiment, all specimens have a thickness of 2 mm with 11 layers of glass fibres. A resulting fibre volume content of 41.2% was determined by weighing the samples before and after burning off the polymer matrix at 550 °C. Using the known densities and the measured mass fractions, the fibre volume fraction was then calculated. The specimens for the quasi-static and fatigue tensile tests have a width of 25 mm and a length of 230 mm including 40 mm tabs on each side for load introduction. This results in a free test volume of 150 ∗ 25 ∗ 2 mm^3, which corresponds to DIN EN ISO 527-4 [26]. The test specimens for compression tests, on the other hand, have a width of 15 mm and a total length of 150 mm, including 67.5 mm long tabs glued on both sides. The resulting free test volume of 15 ∗ 15 ∗ 2 mm^3 is designed against Euler buckling [27]. According to DIN EN ISO 14125 [28], the bending specimens have a width of 15 mm and a length of 60 mm. Fig. 1 gives a schematic representation of the respective specimen geometries and the position/size of the installed misalignments.

In addition to the reference specimens, four different variations in fibre misalignment were created. The four defects are in-plane undulation, wrinkle, fold, and a superposition of in-plane undulation and fold. Furthermore, the misalignments are located at various positions in the thickness direction depending on the load case. For reasons of simplification, the manufacturing process is only described for the construction of the misalignment in the middle layer. Misalignments in other layers were applied congruently. To create out-of-plane undulations, two different methods were used. To reproduce a wrinkle, a glass fibre strip with a width of 10 mm and a thickness of 0.3 mm was laid on the fifth ply. These fibres were orientated in 90° to minimise the effect of additional fibres on mechanical properties. This procedure leads to reproducible undulation angles as can be seen in other studies [29,30]. The second out-of-plane misalignment is a fold, an undulation, which leads to the ply touching itself. To create a fold, the sixth ply was first creased with the help of a steel sheet and then folded back. Then it was bent again with the help of a second steel sheet and aligned back in the original direction. The use of 10 mm wide sheets also results in a fold length of roughly 10 mm. The additional weight of the following layers stabilises the fold and allows the steel sheets to be pulled out. To create a reproducible in-plane undulation, the sixth ply gets a 40 mm cut in the middle and is then pulled to the edge of the RTM mould. More specifically, the ply rim is glued to a GFRP strip, which is likewise glued to a spacer in the mould. This setup allows to vary the amount of undulation by changing cut-length, strip size, or spacer size. In this study, it was used to guarantee a misplacement of 10 mm per side and 20 mm in total. The superposition consists of a fold on the second layer and an in-plane undulation in the sixth layer. The respective misalignments were introduced in the same way as for the individuals. The manufacturing process is described in more detail in a previous study [31].

After plate manufacturing, specimens were cut to size using a high-precision ATM Brillant 265 saw (ATM Qness GmbH, Germany). To avoid shear forces and minimise edge effects, all corners were rectangular and the edges polished.

To ensure that the results obtained are also statistically validated, several specimens per misalignment were tested for each load case. In quasi-static tests, at least five specimens and in fatigue tests, at least two specimens per load level were examined. In addition, specimens were taken from different plates to minimise the risk that the measured values are caused by unintentional defects during the manufacturing process.

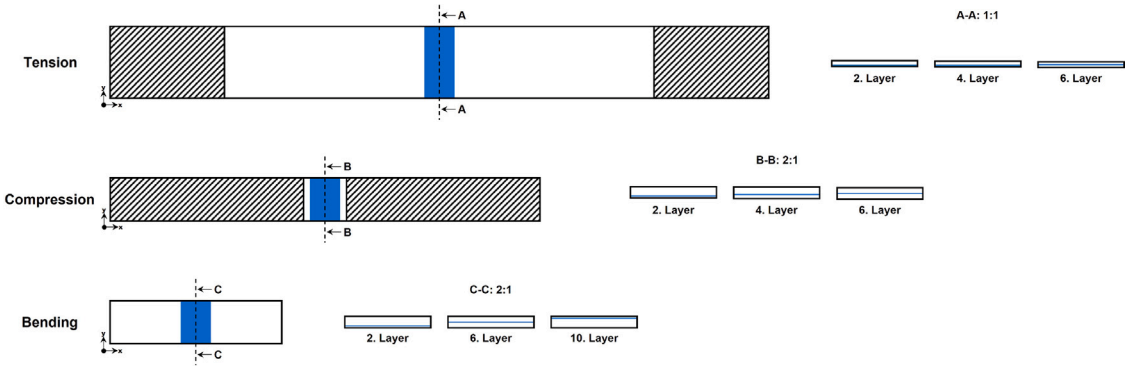

Fig. 1. Schematic representation of specimen geometries displaying the fibre misalignment position (blue) and tabs (striped). (For interpretation of the references to colour in this figure legend, the reader is referred to the web version of this article.)

2.2. Test setup

Before testing, all specimens were dried for 24 h at 40 °C under a vacuum, to minimise the moisture content and stored additional 24 h under testing conditions.

Quasi-static tensile tests were carried out on a 100 kN universal testing machine (ZwickRoell GmbH & Co. KG, Germany) true to DIN EN ISO 527-4 [26]. Hydraulic clamping jaws with 100 bar holding pressure and a multiextensometer for strain measurement were used for the tests. The test speed was 2 mm/min.

Compression tests were performed using a 400 kN universal testing machine (ZwickRoell GmbH & Co. KG, Germany) at a testing speed of 1 mm/min. To avoid slippage, the machine was equipped with hydraulic grips (IMA Dresden, Germany), which gripped the specimen tabs with a pressure of 250 bar. The tests were conducted in accordance with ASTM D6641 [27].

The 3-point bending tests were performed on a 10 kN universal testing machine (ZwickRoell GmbH & Co. KG, Germany). The geometry and the test parameters were selected in accordance with DIN EN ISO 14125 [28]. The support distance was therefore 40 mm, and the test speed 1 mm/min.

The fatigue tests were performed on a universal hydraulic testing machine (Instron-Schenk, Germany) with sinusoidal cyclic loading, equipped with hydraulic grips and a loading capacity of 63 kN. The clamping jaws had a holding pressure of 100 bar, the stress ratio was 0.1 and the frequency was 3 Hz.

3. Visualisation and detection of the introduced fibre misalignments

3.1. Visualisation and description via X-ray CT scan

For a precise and 3D revealing analysis of how misalignments affect the fibre architecture, a high resolution CT-system V|tome|x-L 450 (GE Phoenix X-ray, USA) was used. To achieve visualisation of the entire misalignment area, a 300 kV microfocus X-ray direct beam tube was operated with an accelerating voltage of 90 kV and an electrical tube current of 70 µA. The opposite flat panel detector area was 2006 × 2016 pixels. As a result, a resolution of 20 µm was achieved according to the calibration. Fig. 2 shows the resulting CT scans of representative specimens with fibre misalignments.

The CT scan of the in-plane undulation clearly shows that the corresponding layer is rotated and has a parabola-like shape. The apex is characterised by a lower fibre volume fraction. Next to the apex, the layers form a homogeneous fibre misalignment, in this case with an angle of 53°. This angle is at the upper end to what Riddle et al. [32] measured as typical in-plane undulations in wind turbine blades. It can also be seen that the fibres in this area are more compact compared to not only the resin-rich zones around the apex but also to the defect-free areas. As expected, this misalignment has no influence in the thickness direction as can be seen in the x-z view (red). In the right part of the x-z view, the affected fibres are visible as ellipses, as is usual for diagonal fibre layers.

Regarding the wrinkle, the 10 mm GF strip used for the undulation is clearly visible in the CT scan. In the thickness direction, it can clearly be seen that the 0.3 mm thick strip forces the surrounding layers to be aligned at an 8° angle, resulting in the formation of a resin pocket. The set angle of 8° is one of the most common out-of-plane misalignments in wind turbines [33]. However, the resulting resin pocket in this area is relatively small. Due to the inserted GF strip, the local fibre volume fraction in this region increases accordingly. Ignition loss measurements showed an increase from 41.3% in defect-free areas to 46.1% in the wrinkle region.

The built-in fold is clearly visible in the top view. The touching layers look like a kind of spiral. As the layers lie parallel on top of each other without pressure, they are bent slightly to the side during compaction, resulting in this fibre geometry. It is clear to see, in the thickness direction, that the fold has a very large influence on the fibre architecture and also results in a resin pocket. This resin pocket is significantly larger than that in the wrinkle. In addition, similar to the wrinkle, there is also an out-of-plane undulation of the surrounding layers. Due to the nature of this defect, the effective number of plies increases from 11 to 13 in this region. This effect was also confirmed by ignition loss measurements, showing that the local fibre volume fraction reaches 48.3% in the folded area.

The superposition shows the same characteristics as the single misalignments in-plane undulation and fold. The CT-scan of the sixth layer clearly shows how the fibres shift due to the in-plane undulation. In the thickness direction, the fold, including the resulting resin pocket, is still clearly recognisable. As with the single fold, this defect leads to an increased local fibre volume fraction in the affected region.

3.2. Fibre misalignment detection and characterisation via ultrasonic testing

In addition to investigating the influence of defects on mechanical properties and failure behaviour, the detection of these defects is also of great importance. Due to the influence of fibre misalignments on the directional stiffness, it can be assumed that these defects will also affect the propagation behaviour of acoustic waves. The evaluation of this can therefore be used as a testing approach with which misalignments can be detected non-destructively. Although conventional ultrasonic testing is not suitable for this particular test case, there are two ultrasonic testing methods that can be used to characterise the anisotropic propagation behaviour of elastic waves in composite materials: the phase velocity evaluation of Lamb waves and testing with linear polarised shear waves using the birefringence effect [34].

Lamb waves are elastic waves that propagate within solid plates. They show a dispersive behaviour. The propagation velocity is therefore dependent on the frequency as well as the thickness of the plate, the elastic constants, and the density of the material. Depending on the excitation frequency, two basic modes of Lamb waves occur: symmetric (S) and asymmetric (A) modes.

The phase velocity of the asymmetric A_0-mode can be derived for small ωD approximately from the following equation [35]:

$$v_{A_0} = \sqrt[4]{\frac{E}{3\rho(1-\nu^2)}}\sqrt{\frac{\omega D}{2}} \tag{1}$$

with the young's modulus E, the density ρ, the Poisson's ratio ν, the angular frequency ω and the thickness of the specimen D. As the equation shows, it is possible to estimate small deviations of the young's modulus by measuring the phase velocity v_{A_0}.

The phase velocity of the Lamb waves was measured four times along the longitudinal axis of the specimens using air-coupled ultrasonic testing in a one-sided re-emission arrangement. Such a test setup is very sensitive to the fundamental asymmetric mode of Lamb waves, which is why this mode is used for further considerations. The test setup consisted of two 200 kHz transducers (Ultran Group, USA), a 46 dB low noise amplifier (Inoson GmbH, Germany) and the ultrasonic testing device UltraSCOPE AIR (Dasel SL, Spain). The results of these experimental investigations are shown in Fig. 3.

It can be seen that the defect-free test specimen has the lowest phase velocity v_{A_0} of all specimens. Following Eq. (1), a misalignment-related increase in stiffness can be suggested, as the thickness of the specimen D and the angular frequency ω are identical for all tests performed. This is most likely due to the local increase in the fibre volume content, which is present in the misalignments wrinkle, fold, and superposition as a result of the artificial misalignment preparation. However, the interpretation of the phase velocity of the A_0-mode can be considered as complex, since the expected decrease in tensile or compressive strength cannot necessarily be derived from a misalignment-related local increase in the Young's modulus.

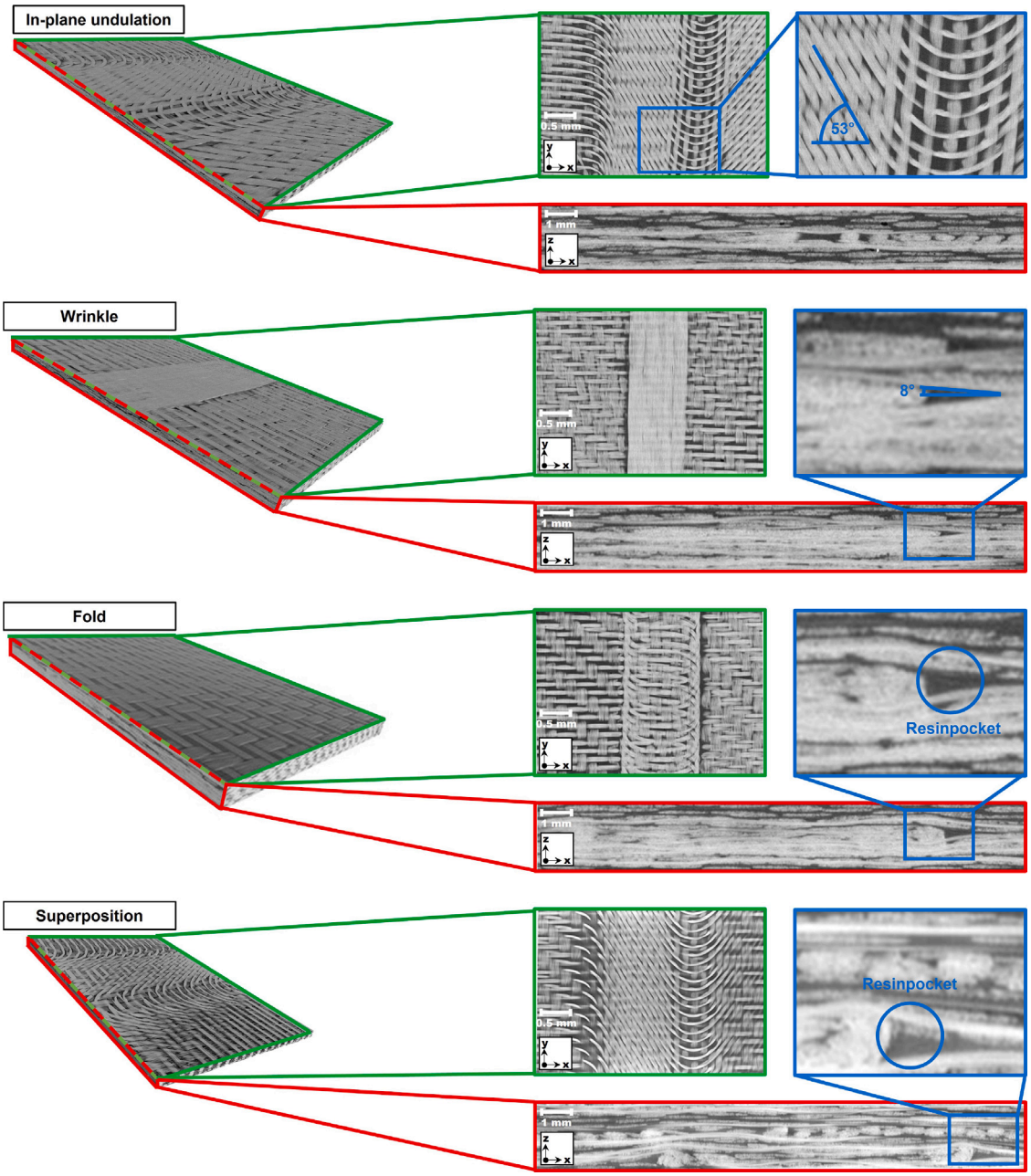

Fig. 2. CT scans in isometric, top (green), and side (red) view of the representative specimens with the investigated fibre misalignments in the middle layer. (For interpretation of the references to colour in this figure legend, the reader is referred to the web version of this article.)

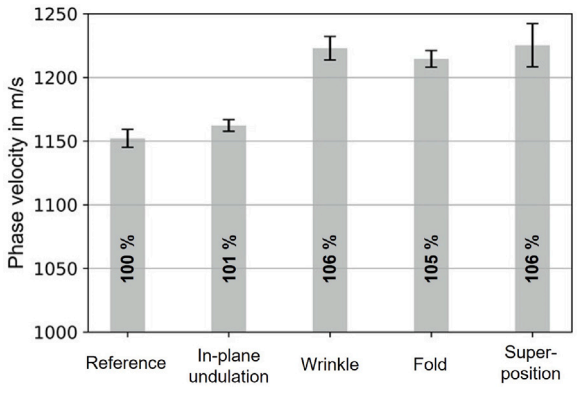

Fig. 3. Phase velocity of the first asymmetric lamb wave mode A_0.

When testing with linear polarised shear waves, the direction-dependent transverse phase velocity was measured along (∥) and transverse (⊥) to the longitudinal axis of the test specimen. The results provide an indication of the stiffness of the laminate, as phase velocities can be analytically calculated with the Eqs. (2), the density ρ, and the directional shear moduli c_{55} and c_{44} derived from the elasticity tensor.

$$v_{t\parallel} = \sqrt{\frac{c_{55}}{\rho}} \qquad and \qquad v_{t\perp} = \sqrt{\frac{c_{44}}{\rho}} \tag{2}$$

In order to characterise the in-plane fibre structure and therefore to detect fibre misalignment, a degree of anisotropy A was calculated with the two-phase velocity according to $A = (1 - \frac{v_{t\perp}}{v_{t\parallel}}) * 100\%$. The experiments were performed with a 1 MHz shear wave transducer (Evident Scientific Inc., Japan) and the ultrasonic testing device RAM-5000 (Ritec Inc., USA). The experimental results are summarised in Table 1:

Table 1
Influence of fibre misalignments on the transversal phase velocity and the degree of anisotropy.

	Reference	In-plane undulation	Wrinkle	Fold	Superposition
$v_{t\parallel}$ in m/s	1299.43	1294.46	1318.55	1424.21	1415.44
$v_{t\perp}$ in m/s	1300.50	1315.63	1363.51	1415.33	1429.98
A in %	−0.08	−1.64	−3.41	0.62	−1.02

In the case of an in-plane undulation, a slight reduction in $v_{t\parallel}$ and an increase in $v_{t\perp}$ can be observed due to the deviation in fibre orientation, resulting in $A < 0\%$. The wrinkle leads to a slight increase in $v_{t\parallel}$ but to a significant increase in $v_{t\perp}$ and thus to $A \ll 0\%$ due to the additional glass fibre layer in the 90° direction. Due to the additional fibres in the fold, a slight increase of both phase velocities can be observed, leading to $A > 0\%$. The superposition results are particularly striking, since they suggest that the anisotropy of misalignments can be summed up, as demonstrated by the combination of the misalignments in-plane undulation and fold in the superposition test specimen.

4. Experimental results and discussion

4.1. Quasi-static tensile tests

In order to gain a general understanding of the influence of misalignments on the mechanical behaviour of GFRP, quasi-static tensile tests were carried out. Fig. 4 shows the individual strengths and stiffnesses.

It can surprisingly be seen for the stiffnesses (Fig. 4 (left)) that the reference specimens have the lowest stiffness at 23.6 GPa, while the specimens with an in-plane undulation have, with 24.1 GPa, only a slightly higher stiffness. The fold and the superposition lead to stiffnesses of 24.9 GPa and 25.0 GPa and the wrinkle even results in a stiffness of 26.1 GPa. Therefore, misalignments, especially in specimens with out-of-plane undulations, result in stiffnesses higher than that of the reference specimens. However, the increase is with 5% for the fold, 6% for the superposition, and 11% for the wrinkle still within the range of standard deviations. According to Wu et al. [36], little to no stiffness reduction was found, while other studies [33,37] measured a decrease in stiffness caused by misalignments. At first sight, such a reduction also seems comprehensible, but one possible explanation lies in the fibre architecture of the misalignments. The additional fibres that produce the undulations in the thickness direction, namely wrinkle and fold, lead to a higher local fibre volume content. The measurement of elongation on the Z100 testing machine was carried out using a multi-extensometer. The elongation, and therefore the stiffness, is measured by the relative displacement of two blades in relation to each other. The blades are 50 mm apart by default. As a result, changes in elongation in this area are taken more into account. Therefore, it can be assumed that the measured differences between the various configurations are significantly smaller over the entire size of the test specimen. However, it can be seen that, in terms of stiffness, there appears to be a conflict between the 'ideal' fibre orientation and a higher fibre volume fraction. This apparently leads not only to no reduction, but in extreme cases even to an increase in local stiffness, which is in line with the results obtained via NDT methods in Section 3.2.

Looking at the strength values in Fig. 4 (right), it can be seen that the reference specimens have the highest strength of 467.9 MPa. The in-plane undulation and wrinkle lead to relatively similar strength values of 429.7 MPa and 428.1 MPa. The fold's strength is slightly lower with 420.0 MPa and even though this is the highest strength reduction of all individual misalignments it is still relatively moderate because the resin pocket is not so relevant under tensile loading [30]. The strength reductions of the specimens with a single misalignment are in the range between 9 and 11%, which corresponds almost exactly to the number of plies that are directly affected, which is also 1/11 ~9%. Therefore, a misalignment leads to at least the reduction in strength by the relative volume fraction of the affected layer. However, a reduction in strength of 32% to 318 MPa occurred with the superposition of misalignments. This reduction is even higher than the simple addition of the individual reductions of in-plane undulation and fold. A combination of several misalignments leads to increased stress concentrations in the laminate and, as a result of the occurrence of the fold outside the centre layer, to residual stresses in the laminate. These aspects favour damage initiation and growth and could explain the very high reduction in strength. With regard to the stress concentration, it can also be seen that most of the specimens tested broke in and around the misalignment. The crack has either grown through the test specimen at the misalignment or has previously spread within the misalignment, as shown in Fig. 5. No further change was observed between the damage behaviour of the defect-free specimens and the specimens with misalignments or within the specimens with misalignments.

The mechanical results obtained are difficult to directly compare with other values in the literature, as there are a high number of factors (stacking sequence, type and size of the misalignment, etc.) that influence the reduction in strength. A good overview of characteristic values can be found in Kulkarni et al. [38]. Tests with in-plane undulations have shown strength reductions between 10 and 15% [36,37,39,40]. For wrinkles, literature values vary widely, ranging from about 14% to

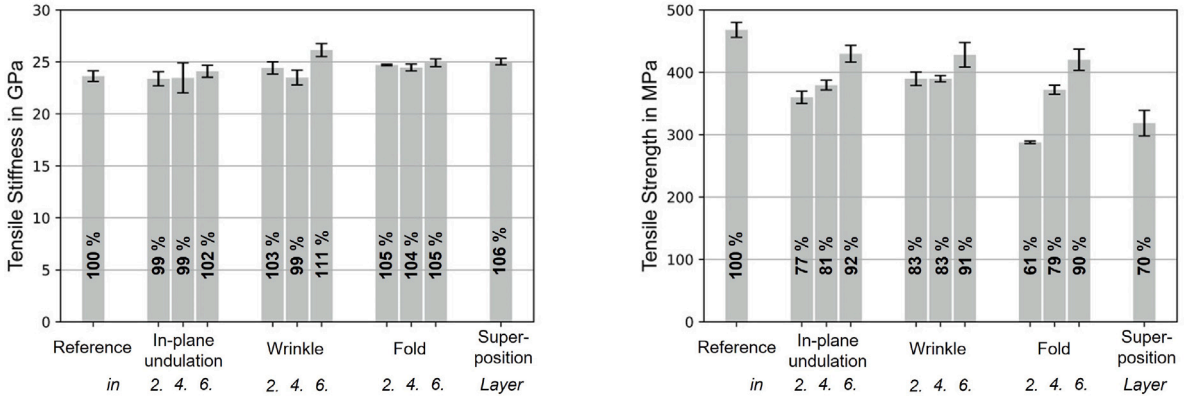

Fig. 4. Tensile stiffnesses (left) and strengths (right) of specimens with and without fibre misalignments.

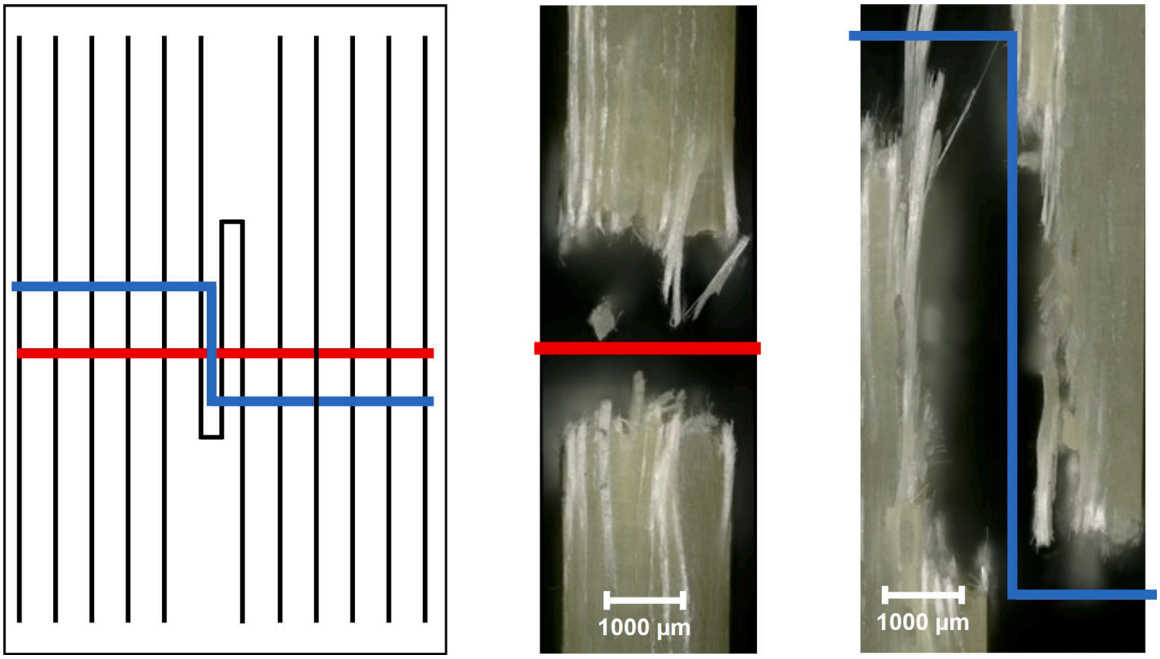

Fig. 5. Failure modes after quasi-static tensile tests for representative specimens with fibre misalignments. Failure occurs either through the misalignment (red) or along/parallel to the misalignment (blue). (For interpretation of the references to colour in this figure legend, the reader is referred to the web version of this article.)

over 25% [33,41]. Woigk et al. [42] also investigated superpositions and found that a combination of misalignments can be more critical than the sum of the individual misalignments. The results of this study are consistent with this general observation.

4.2. Quasi-static compression tests

Fig. 6 shows the results of the quasi-static compression tests. The stiffnesses are shown on the left part of the figure. For most misalignments, no significant drop in stiffness can be recognised between the reference specimens and the misalignment types. As an exception, in-plane undulations are affected to a small extent, which is basically to be expected, as these effectively have one ply in which parts of the fibres are no longer in the 0° direction, but at an angle of 55°. The other configurations show no reduction in stiffness, or in some cases even an increase. This observation is initially unintuitive and does not agree with most values in the literature, which have found a reduction in stiffness as a consequence of imperfections [40,43,44]. However, on closer inspection, the results are understandable as these imperfections are caused by additional fibres and a higher local fibre volume content, as described in the previous section.

The strength values are shown on the right-hand side of the Fig. 6. First, it is clear to see that the reference specimens have the highest strength with 354.7 MPa. Normally, the failure of compression test specimens is divided into four steps: uniform deformation, elastic buckle, kink band, and shear failure. The misalignments favour local buckling and thus accelerate the usual growth of damage [45]. For this reason, it is only logical that misalignments reduce the strength. For specimens with in-plane undulations, it can be seen that they yield a lower strength, regardless of the position of the misalignment. It can also be seen that the reduction in strength decreases when the misalignment is more centred (in relation to the thickness). The respective strength values are 306.4, 290.9, and 280.6 MPa. This behaviour is expected, as the misalignment is better supported deeper in the specimen [46]. Misalignments close to the edge of the specimen favour early initiation of damage and, as a consequence, local buckling, which ultimately leads to global failure. Both the wrinkle with 286.1, 264.0, 309.8 MPa (outside to centre) and the fold with 235.1, 224.9, 270.1 MPa lead to significantly reduced strength values. However, they do not follow the same trend as the in-plane undulation with respect to the dependency between strength and misalignment position. In these configurations, the minimum strength is when the misalignment in the fourth layer and not on the edge. Microscopy images of specimens with out-of-plane undulations in the second or sixth layer, which are not shown here due to lack of space, show that the misalignment on the second layer is ‘restricted’ in thickness direction due to the mould and can therefore negatively affect fewer layers. The misalignment is more critical if more layers are undulated due to provoked microbuckling [47]. The misalignment on the fourth layer appears to represent the ‘optimum’, in which as many layers as possible are influenced, but the asymmetrical behaviour of the material and the resulting local buckling still occurs. In the case of the superposition, the strength value is reduced to 247.2 MPa. The strength reductions are generally higher than those in the tensile tests. Compression therefore appears to be more critical as a load case for areas with misalignments, presumably due to the microbuckling already mentioned. However, no differences between the various configurations can be deduced regarding the failure modes of the different specimens due to the relatively small free test volume.

Similar to the tensile results, a direct comparison of the measured influence of misalignments on mechanical properties with other studies is challenging due to significant variations in misalignment size and fibre layup. Kulkarni et al. [38] provide a useful overview of typical ranges reported in the literature. For example, Mandell et al. [37] investigated in-plane undulations in quasi-isotropic carbon fibre-reinforced polymers (CFRP) and reported a strength reduction of 13%. Adams et al. [48] found that an in-plane undulation could reduce the strength by up to 30% in GFRP specimens. Similarly, wrinkles in CFRP cross-ply laminates have been shown to cause strength reductions of up to 35% when 33% of the plies are affected [43]. Mukhopadhyay et al. [40] demonstrated that in quasi-isotropic CFRP, waviness angles of 5.6°, 9.9°, and 11.4° resulted in strength reductions of 18, 33.5, and 32.9%, respectively. Nimbal et al. [44] reported similar reductions (31.3%) for

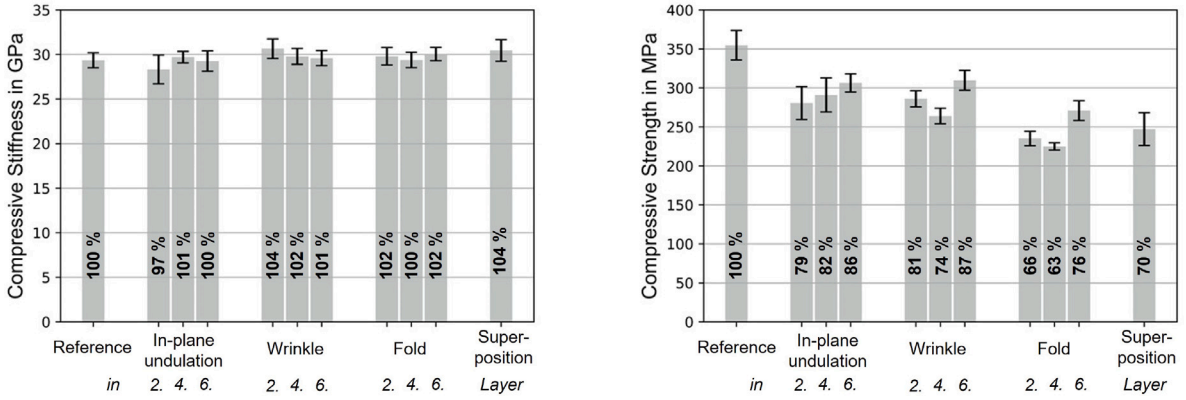

Fig. 6. Compressive stiffnesses (left) and strengths (right) of specimens with fibre misalignments in different layers compared to defect-free specimens.

unidirectional lamina. In the study by Adams et al. [49], 20% of the load-bearing fibres were affected instead of 1/11 directly, which led to a strength reduction between 12 and 14% for the same aspect ratio.

4.3. Quasi-static three-point bending tests

Bending tests result in a linear strain distribution throughout the thickness of the test specimen. Compressive stresses are formed on the upper side of the specimen and tensile stresses on the lower side. The maxima of these stresses are found on the surface and the centre layer has no tensile or compressive stresses but the maximum shear stresses. In this study, the misalignment position is counted from the bottom of the test specimen. For example, in-plane undulation in the second layer therefore means that the in-plane undulation is on the tension side.

It can be seen in Fig. 7 (left) that the reference specimens and specimens with an in-plane undulation in the sixth layer have almost the same stiffnesses with 22.4 and 21.9 GPa respectively. Since the misalignment is in the neutral position, this is expected. Otherwise, in-plane undulations lead to a reduction in stiffness on both the compression (16.8 GPa) and tension (18.0 GPa) sides. The wrinkle in the centre of the test specimen results in a higher stiffness of 23.1 GPa. This is in accordance with Steiner's theorem, because the load-bearing layers are displaced further outward. Unfortunately, the standard deviation is relatively high for the wrinkle on layers two and ten, but it can still be seen that this leads to reduced stiffnesses of 21.2 and 21.1 GPa. However, this change is smaller than for the in-plane undulations, presumably because more fibres lie in the area of the maximum deflection. The stiffness of specimens with folds in the centre layer is, also due to Steiner's theorem, increased to 25.1 GPa. In addition, the specimens with an off-centre fold still have a similar stiffness to the reference specimens with the fold in the second layer to result in 23.5 GPa and in tenth layer 22.8 GPa. As in the previous tests, this may also be due to the locally higher fibre volume fraction.

Analogous results emerge for the strength values (Fig. 7 (right)). The reference specimens and specimens with an in-plane undulation in the centre have with 508.4 MPa and 509.1 MPa almost identical strength values. Out-of-plane undulations like the wrinkle, and the fold at the 'ideal' position in the centre lead to an increase in strength up to 521.1 and 545.4 MPa. Otherwise, all misalignments outside of the centre layer lead to a reduction in flexural strength. It is also recognisable that it is more critical for all misalignment types if the misalignment is on the tensile side (2. layer) than on the compression side (10. layer). However, since the reference specimens also fail on the tensile side, this observation is understandable as defects lead to a stress concentration in addition to the usual load. Depending on the test specimen, the damage has grown to different depths in the test specimen. Fig. 8 clearly shows, for a specimen with a fold on the tension side, that a crack runs through the test specimen at the fold or through the resin pocket directly next to it. In contrast to the quasi-static tensile test, the crack follows the contour of the defect very precisely, although the defect is not located at the point of maximum deflection. This defect weakens the fibre architecture to such an extent that crack initiation does not take place at the point of highest elongation. Even if there is a clear reduction in strength in the two other types of misalignments, the associated damage patterns differ only slightly from the reference specimens.

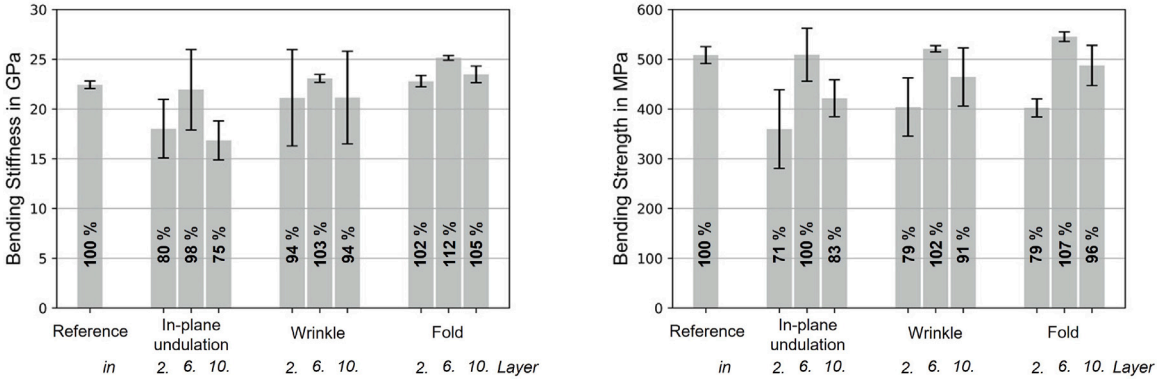

Fig. 7. Bending stiffnesses (left) and strengths (right) of specimens with fibre misalignments in different layers compared to defect-free specimens.

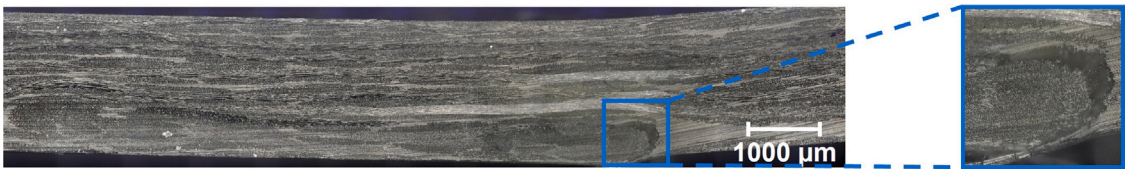

Fig. 8. Failure during bending test of a specimen with a fold on the tension side. Fracture through the resin pocket close to the fold; highlighted and zoomed in.

In the current test, the misalignments was centred under the load application. It can be assumed that the strength reductions will be even greater if the test specimens are positioned so that the edge of the imperfection overlaps with the maximum strain.

Although the literature provides limited data on the effect of misalignments on flexural behaviour, Allison et al. [50] reported a strength reduction of 26% for localised wrinkles. During four-point bending tests, in another paper [11], it was concluded that misalignments on the tensile side are more critical, and wrinkles of a comparable misalignment size showed a strength reduction of ≈15%.

4.4. Numerical investigation of in-plane undulations

In order to investigate the theoretical influence of in-plane undulations on the quasi-static strength and stiffness of fibre-reinforced polymers, a numerical framework was implemented in Abaqus/Explicit and compared with the experimental results. For the simulation of tensile and compressive loading, the geometric model was constructed according to the dimensions shown in Fig. 1. The laminate was discretised using continuum shell elements (SC8R), with each layer represented by a separate set of these elements. The layers were stacked to replicate the multi-layered structure of the composite material. In the region representing the misalignment, one layer rotation is incrementally rotated to model the effect of in-plane fibre misalignment of the laminate (see Fig. 9). A complete 45° shift of the layer represents the most significant impact and thus serves as the "worst-case" scenario. As in the experimental procedure, the impact of the through-thickness position of the defective layer was varied to comprehensively assess its effect on the mechanical properties of the laminate.

To accurately capture the constitutive behaviour of the fabric, the well-established continuum damage model Abq_Ply_Fabric [51] was used as the material model. This model was accessed via a built-in VUMAT subroutine in Abaqus/Explicit. It is particularly well-suited for simulating progressive damage, stiffness degradation, and plasticity effects under a wide range of loading conditions for fabric composites. Here, the elastic behaviour was modelled as orthotropic and defined in a local coordinate system aligned with the principal fibre directions. The material description incorporated progressive damage mechanisms in both the fibres and the matrix, employing distinct damage variables for tensile and compressive failure modes along the fibre directions, as well as for shear-induced matrix cracking. The evolution of damage is captured by the intra-laminar fracture energies given as material properties, ensuring consistent energy dissipation during failure. Additionally, the subroutine captures a non-linear shear response, which reflects the plastic deformation and stiffness degradation of the matrix under shear loading. This response is characterised by a yield function, a hardening law, and the associated evolution of damage. For a detailed explanation of the underlying principles and mechanisms of the material model, the reader is referred to [51].

To ensure accurate results, the model calibration was mostly based on standard experimental procedures. The shear damage needs to be calibrated using cyclic tensile tests on ±45° laminates, ensuring an accurate representation of the matrix's contribution to the plastic composite behaviour. However, while the strength and elasticity parameters were determined experimentally, the shear parameters and

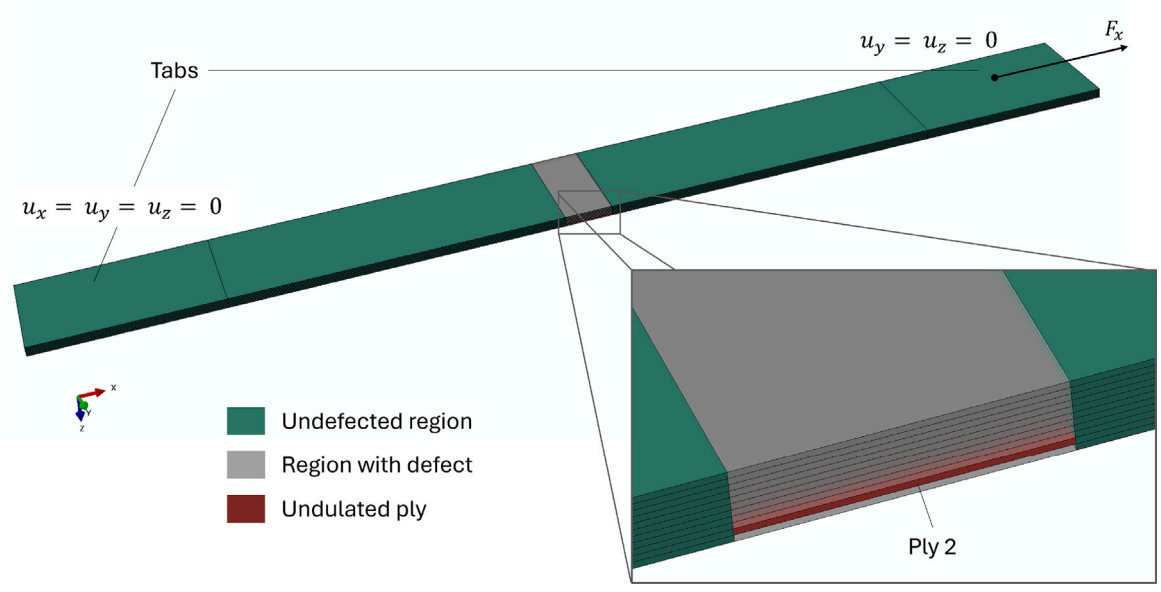

Fig. 9. Schematic representation of the finite element model, exemplified for the tension load case of an in-plane undulation in the second layer.

Table 2
Material parameters for the continuum damage model.

Parameter	Description	Value	Source
E_1^+	Tensile modulus in fibre direction 1	22.4 GPa	Experiment
E_1^-	Compressive modulus in fibre direction 1	22.4 GPa	Experiment
E_2^+	Tensile modulus in fibre direction 2	22.4 GPa	Experiment
E_2^-	Compressive modulus in fibre direction 2	22.4 GPa	Experiment
$\nu_{12}^+ = \nu_{12}^-$	Poisson's ratio	0.232	[52]
G_{12}	Shear modulus	6.2 GPa	[52]
X_1^+	Tensile strength in fibre direction 1	465 MPa	Experiment
X_1^-	Compressive strength in fibre direction 1	351 MPa	Experiment
X_2^+	Tensile strength in fibre direction 2	465 MPa	Experiment
X_2^-	Compressive strength in fibre direction 2	351 MPa	Experiment
G_f^{+1}	Fracture energy (tension, direction 1)	100 kJ/m^2	[53]
G_f^{-1}	Fracture energy (compression, direction 1)	85 kJ/m^2	[53]
G_f^{+2}	Fracture energy (tension, direction 2)	100 kJ/m^2	[53]
G_f^{-2}	Fracture energy (compression, direction 2)	85 kJ/m^2	[53]

intra-laminar fracture energies of this material were approximated for simplicity from literature values [52,53]. The complete set of material parameters and their sources are listed in Table 2.

Numerical results

The numerical results, depicted in Fig. 10, indicate a reduction in strength of up to approximately 3.5% in the most-critical 45° misalignment for both the tensile and compressive loading cases. In the tensile loading case, the reduction in strength is almost independent of the through-thickness position, whereas in the compressive loading case, a significant dependence on position is observed, with off-centre misalignments causing more significant reductions in strength in low rotation angles. Nevertheless, the simulated strength values for tension and compression remain in a comparable range. However, compared to values of up to 20% in the experimental results (see Figs. 4 and 6), the strength reduction observed in the simulation is significantly smaller.

This discrepancy can be attributed to several simplifying assumptions in the numerical model:

- Stress concentrations: Although the model accounts for angular misalignments in the laminate structure, due to its macroscopic nature, it does not capture local stress concentrations in the microstructure.
- Fibre orthogonality in rotated structures: In the simulation, the fibres within the fabric remain orthogonal during rotation, which does not necessarily reflect the behaviour in a real misalignment. In practice, the fibre bundles may shear against each other to some extent, resulting in non-orthogonal structures.
- Neglect of resin-rich zones: Resin-rich zones as localised inhomogeneities significantly contribute to the variability in material strength and directly impact the load transfer mechanisms between the fibres and the surrounding matrix. In the case of this misalignment, resin-rich zones are particularly prevalent as the fibre layers are pulled outward during the manufacturing process, further exacerbating these effects.
- Omission of residual stresses: Residual stresses due to shrinkage and cooling during the manufacturing are not included in the model. These stresses can significantly affect the stress distribution and consequently the resulting strength.

The discrepancy between numerical and experimental results highlights the inherent limitations of approximation models in homogenising the effects of misalignments. Even under conservative assumptions of larger angular misalignments than those typically observed in practice, the simulated strength reductions remain lower than those found experimentally. While the effect of shearing of fibre bundles appears to be small, this discrepancy points to the importance of local stress concentrations, particularly in resin-rich zones and due to residual stresses. These factors play a critical role in the material response and cannot be adequately represented in homogenisation models. This result is in line with other research (e.g. [54]), where analytical models often fail to accurately predict strength values for different local and global fibre volume fractions. This challenge is particularly pronounced in the present study, where the moderate fibre volume fraction of 41.2% further amplifies the discrepancies between the local and global strength behaviour.

In summary, the simulation successfully captures the fundamental trend of strength reduction, but the simplified assumptions used in homogenising misalignments result in an overestimation of strength. This result highlights the need for improved modelling of local damage mechanisms.

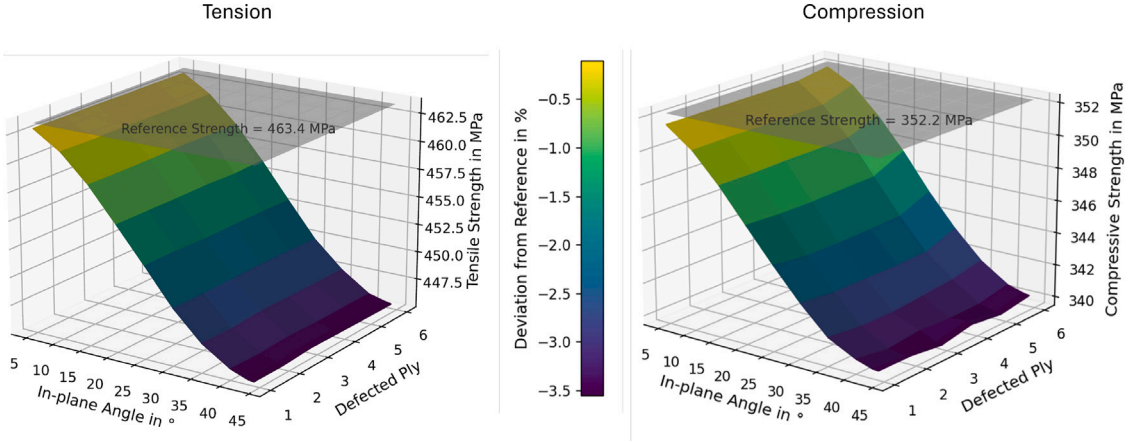

Fig. 10. Tensile (left) and compressive (right) strength as a function of the in-plane rotation angle and the through-thickness position.

4.5. Fatigue tests under tensile load

In fatigue tests, the specimen is repeatedly loaded below its quasi-static strength. Cyclic loading makes it possible to gain a better understanding of the initiation and growth of damage within the specimens. If they are not sorted out or repaired due to their defect, real parts are used like defect-free parts and must therefore withstand the same loads. For this reason, this paper compares the lifetimes of the various misalignments as a function of the absolute amplitudes. Fig. 11 shows the S–N curves for the various configurations.

As expected, the reference specimens withstand, at the same absolute load level, more cycles than the specimens with fibre misalignments. The misalignments and the previously mentioned stress concentrations lead to a reduction in service life. The in-plane undulation, which was most similar to the defect-free specimens in terms of static properties is also most similar to them in terms of service life. At very high and medium loads, the service life is still almost identical, but this can be partly attributed to the low outlier value of the defect-free specimens. At low load levels, the difference between the defect-free specimens and those with in-plane undulations becomes clearer. At a medium load of 235 MPa, the reference specimens can withstand ≈9000 cycles, whereas the specimens with in-plane undulations can only withstand ≈6000 cycles, which corresponds to a reduction in service life of 33.3%. This drastic reduction can be explained by the fact that, due to the in-plane undulation, there is effectively one fibre layer less to take up the occurring stresses, which means that the other layers are forced to withstand more of the load. The course of the S–N curve for specimens with wrinkles is similar to those with in-plane undulations. In this case, a reduction in service life occurs at higher load levels, while the curve approaches the reference curve again at lower stresses. For both of these types of misalignment, it can be said that, taking into account the standard deviation within the specimens and the only slightly lower strength values, there is probably a slight shift to the left compared to the reference specimens, meaning a small to medium reduction in service life. For specimens that contain a fold, the S–N curve is clearly shifted to the left, which corresponds to a sharp reduction in service life. At a load level of 235 MPa, for example, this type of misalignment can only withstand an average of 1750 load cycles, which means a reduction in service life of 80% compared to the reference specimens. The main reason for this sharp reduction is the resin pocket, which is formed during the manufacturing process and can be seen in Fig. 2. There is a stress concentration at the fold and this is most likely where the crack initiation takes place. The cyclic loading leads to cracks in the resin pocket and ultimately to a complete failure of the test specimen. As expected, the combination of two types of misalignment, the superposition, has the lowest lifetime of all configuration. At the high load levels, the specimens only withstand a few load cycles, as this already corresponds to their quasi-static strength. However, these specimens also withstand comparatively few load cycles at all other load levels. At 235 MPa, for example, there are only ≈500 cycles on average, which corresponds to a reduction in service life of around 94%. The specimen configuration fails so quickly because the damage mechanisms of the other misalignment types can occur here in combination and simultaneously. On the one hand, the effective number of layers that can carry loads is reduced due to the in-plane undulation, which is why all other layers are more heavily loaded. Furthermore, there is a stress concentration in and around the resin pocket, which is problematic for crack initiation and growth. In contrast to the fold specimens, the fold is not in the centre of the specimen and is therefore supported by fewer layers, which also allows for earlier failure.

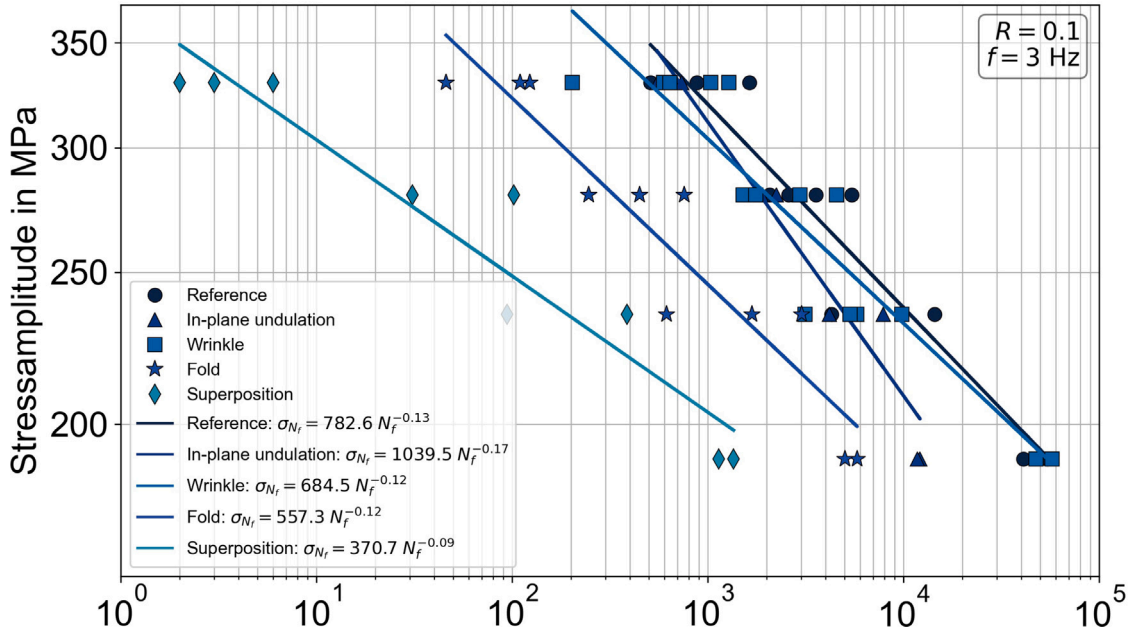

Fig. 11. S–N curve of specimens with and without fibre misalignments.

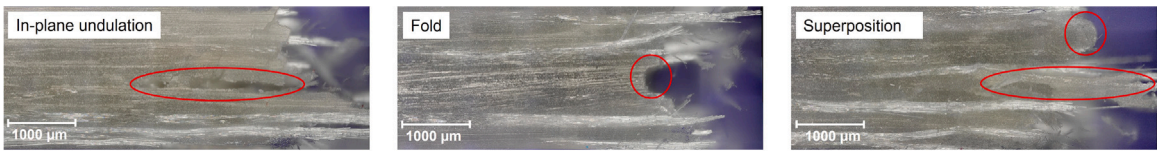

Fig. 12. Damage of representative fatigue specimens after failure.

The specimens with wrinkles do not show a particular unusual damage pattern and behave similarly to the reference specimens even-though the fracture always occurs close to the inserted GF-strip. But it is possible to describe the failure mechanism of the other types of misalignments in more detail, using the damage images in Fig. 12.

In the case of specimens with an in-plane undulation, it can be seen from the fracture surfaces that an approximately 15 mm fibre bundle is pulled from the composite in the middle layer. The position indicates that these are the undulated fibres and that the excessive stress at the radius, at which the in-plane undulation is introduced, leads to a detachment fracture of the fibres and ultimately to their separation. The damage pattern of specimens with a fold show the aforementioned resin pocket. It detached completely from the opposite side during the cyclic test and is still visible after complete failure. Stress increases in the resin pocket, as well as the proportionally worse properties of the resin, lead to cracks, delaminations, and fractures at the resin-fibre interface and eventually to debonding [55,56]. The superposition is the combination of the in-plane undulation and the fold and therefore damage patterns can be found for both types of misalignments. Here, too, the middle layer is torn out at the in-plane undulation, and a fracture occurs in the resin pocket, which reproduces its contour.

5. Conclusion

In this experimental and numerical study, GFRP cross-ply laminates with eleven fibre layers were manufactured in tailored ways to introduce misaligned fibres at different positions. A total of four different types of misalignments were examined: in-plane undulation, wrinkle, fold, and superposition of in-plane undulation and fold. The following findings can be derived from the experimental and numerical results and the associated discussion:

(1) Fibre misalignments can be detected non-destructively by measuring phase velocities of Lamb or shear waves, as stiffness deviations correlate well with quasi-static tensile and compression tests. Shear wave analysis also indicates that multiple misalignments may superimpose.
(2) Fibre misalignments significantly reduce the quasi-static strength of GFRP laminates, with greater losses for bending and compression than for tension. The Young's modulus remains largely unaffected.
(3) The position of a misalignment strongly influences failure behaviour and strength; defects near the laminate edge have a higher impact, but for out-of-plane undulations this effect is limited by the number of affected plies.
(4) Under cyclic loading, misalignments alter the damage mode and cause a substantial decrease in service life, with reductions ranging from at least 33.3% up to 94%.
(5) Finite element models that use homogenised misalignment descriptions fail to capture local geometric imperfections and mesoscopic effects such as fibre-rich or resin-rich zones and residual stresses, leading to an overestimation of mechanical performance.

CRediT authorship contribution statement

Jonas Drummer: Writing – original draft, Visualization, Methodology, Investigation, Formal analysis, Conceptualization. **Tim Luplow:** Writing – original draft, Visualization, Methodology, Investigation, Formal analysis, Conceptualization. **Linus Littner:** Writing – original draft, Methodology, Investigation. **Richard Protz:** Writing – original draft, Visualization. **Sebastian Heimbs:** Writing – review & editing, Supervision, Project administration, Methodology, Funding acquisition. **Marc Kreutzbruck:** Writing – review & editing, Supervision, Methodology, Funding acquisition. **Maik Gude:** Writing – review & editing, Supervision, Project administration, Funding acquisition. **Bodo Fiedler:** Writing – review & editing, Supervision, Project administration, Methodology, Investigation, Funding acquisition, Conceptualization.

Declaration of competing interest

The authors declare that they have no known competing financial interests or personal relationships that could have appeared to influence the work reported in this paper.

Acknowledgements

This research is part of the PAK 988 project with the subprojects 428326921, 428328210, 428323347 and 428324840 of the German Research Foundation (DFG). The financial support of the California Department of Fish and Game, United States is appreciated. Publishing fees supported by Funding Programme Open Access Publishing of Hamburg University of Technology (TUHH).

Data availability

Data will be made available on request.

References

[1] M. Pervaiz, S. Panthapulakkal, M. Sain, J. Tjong, Emerging trends in automotive lightweighting through novel composite materials, Mater. Sci. Appl. 07 (2016) http://dx.doi.org/10.4236/msa.2016.71004.
[2] R. Wiser, J. Rand, J. Seel, P. Beiter, E. Baker, E. Lantz, P. Gilman, Expert elicitation survey predicts 37% to 49% declines in wind energy costs by 2050, Nat. Energy 6 (5) (2021) 555–565, http://dx.doi.org/10.1038/s41560-021-00810-z.
[3] J.M. Lawrence, K.-T. Hsiao, R.C. Don, P. Simacek, G. Estrada, E. Sozer, H.C. Stadtfeld, S.G. Advani, An approach to couple mold design and on-line control to manufacture complex composite parts by resin transfer molding, Compos. Part A: Appl. Sci. Manuf. 33 (7) (2002) 981–990, http://dx.doi.org/10.1016/S1359-835X(02)00043-X.
[4] U. Fasel, D. Keidel, L. Baumann, G. Cavolina, M. Eichenhofer, P. Ermanni, Composite additive manufacturing of morphing aerospace structures, Manuf. Lett. 23 (2020) 85–88, http://dx.doi.org/10.1016/j.mfglet.2019.12.004.
[5] G. Struzziero, J. Teuwen, Residual stresses generation in ultra-thick components for wind turbine blades, Procedia CIRP 85 (2019) 8–12, http://dx.doi.org/10.1016/j.procir.2019.09.002.
[6] D. Kugler, T.J. Moon, Identification of the most significant processing parameters on the development of fiber waviness in thin laminates, J. Compos. Mater. 36 (12) (2002) 1451–1479, http://dx.doi.org/10.1177/0021998302036012575.
[7] K. Mizukami, Y. Mizutani, A. Todoroki, Y. Suzuki, Detection of in-plane and out-of-plane fiber waviness in unidirectional carbon fiber reinforced composites using eddy current testing, Compos. Part B: Eng. 86 (2016) 84–94, http://dx.doi.org/10.1016/j.compositesb.2015.09.041.
[8] P.P. Parlevliet, H.E. Bersee, A. Beukers, Residual stresses in thermoplastic composites – a study of the literature. Part III: Effects of thermal residual stresses, Compos. Part A: Appl. Sci. Manuf. 38 (6) (2007) 1581–1596, http://dx.doi.org/10.1016/j.compositesa.2006.12.005.
[9] M. Thor, M.G.R. Sause, R.M. Hinterhölzl, Mechanisms of origin and classification of out-of-plane fiber waviness in composite materials—A review, J. Compos. Sci. 4 (3) (2020) 130, http://dx.doi.org/10.3390/jcs4030130.
[10] E. Kunze, S. Galkin, R. Böhm, M. Gude, L. Kärger, The impact of draping effects on the stiffness and failure behavior of unidirectional non-crimp fabric fiber reinforced composites, Materials 13 (13) (2020) 2959, http://dx.doi.org/10.3390/ma13132959.
[11] K. Potter, B. Khan, M. Wisnom, T. Bell, J. Stevens, Variability, fibre waviness and misalignment in the determination of the properties of composite materials and structures, Compos. Part A: Appl. Sci. Manuf. 39 (9) (2008) 1343–1354, http://dx.doi.org/10.1016/j.compositesa.2008.04.016.
[12] M.R.L. Gower, R.M. Shaw, W.R. Broughton, Thick composites: Part I:Mechanical test review, part II: Cure optimisation, 2008-04, URL: http://eprintspublications.npl.co.uk/id/eprint/4135.
[13] Y. Fu, X. Yao, A review on manufacturing defects and their detection of fiber reinforced resin matrix composites, Compos. Part C: Open Access 8 (2022) 100276, http://dx.doi.org/10.1016/j.jcomc.2022.100276.
[14] M.R. Wisnom, J.W. Atkinson, Fibre waviness generation and measurement and its effect on compressive strength, J. Reinf. Plast. Compos. 19 (2) (2000) 96–110, http://dx.doi.org/10.1177/073168440001900201.
[15] M. Thor, U. Mandel, M. Nagler, F. Maier, J. Tauchner, M.G.R. Sause, R.M. Hinterhölzl, Numerical and experimental investigation of out-of-plane fiber waviness on the mechanical properties of composite materials, Int. J. Mater. Form. 14 (1) (2021) 19–37, http://dx.doi.org/10.1007/s12289-020-01540-5.

[16] V. Gigante, L. Aliotta, V.T. Phuong, M.B. Coltelli, P. Cinelli, A. Lazzeri, Effects of waviness on fiber-length distribution and interfacial shear strength of natural fibers reinforced composites, Compos. Sci. Technol. 152 (2017) 129–138, http://dx.doi.org/10.1016/j.compscitech.2017.09.008.

[17] J. O'Donnell, V. Chalivendra, A. Hall, M. Haile, L. Nataraj, M. Coatney, Y. Kim, Electrical and shear constitutive response of conductive glass fibre/epoxy composites, Plast. Rubber Compos. 49 (3) (2020) 108–115, http://dx.doi.org/10.1080/14658011.2019.1711345.

[18] M.Y.M. Zaghloul, M.M.Y. Zaghloul, M.M.Y. Zaghloul, Physical analysis and statistical investigation of tensile and fatigue behaviors of glass fiber-reinforced polyester via novel fibers arrangement, J. Compos. Mater. 57 (1) (2022) 147–166, http://dx.doi.org/10.1177/00219983221141154.

[19] M.P. Alves, C.A. Cimini Junior, S.K. Ha, Fiber waviness and its effect on the mechanical performance of fiber reinforced polymer composites: An enhanced review, Compos. Part A: Appl. Sci. Manuf. 149 (2021) 106526, http://dx.doi.org/10.1016/j.compositesa.2021.106526.

[20] J. Lee, C. Soutis, A study on the compressive strength of thick carbon fibre–epoxy laminates, Compos. Sci. Technol. 67 (10) (2007) 2015–2026, http://dx.doi.org/10.1016/j.compscitech.2006.12.001.

[21] M. Ashir, A. Nocke, C. Cherif, Effect of the position of defined local defect on the mechanical performance of carbon-fiber-reinforced plastics, Autex Res. J. 19 (1) (2019) 74–79, http://dx.doi.org/10.1515/aut-2018-0034.

[22] W.B. Hillig, Effect of fibre misalignment on the fracture behaviour of fibre-reinforced composites, J. Mater. Sci. 29 (2) (1994) 419–423, http://dx.doi.org/10.1007/BF01162501, URL: https://link.springer.com/article/10.1007/bf01162501.

[23] L.E. de Castro Saiki, G.F. Gomes, Understanding and mitigating delamination in composite materials: A comprehensive review, Mech. Adv. Mater. Struct. 31 (30) (2024) 13147–13167, http://dx.doi.org/10.1080/15376494.2024.2333490.

[24] J. Drummer, D. Gibhardt, J. Körbelin, B. Fiedler, General influence of the environmental temperature on the matrix strength under tensile and compressive loading - a comprehensive study on high performance matrices, Compos. Sci. Technol. 230 (4) (2022) 109486, http://dx.doi.org/10.1016/j.compscitech.2022.109486.

[25] Valmiera Glass Group, T-glasgewebe 92125 e glass fabric technical data sheet, version 2.0, 2018, URL: https://shop.swiss-composite.ch/shop/resources/downloads/t-glasgewebe-92125-valmiera-e.pdf. (Accessed 23 June 2025).

[26] Deutsches Institut für Normung, DIN EN ISO 527-4, plastics - determination of tensile properties. Part 4, test conditions for isotropic and orthotropic fibre-reinforced plastic composites, 2022.

[27] ASTM International, ASTM D6641, standard test method for compressive properties of polymer matrix composite materials using a combined loading compression (CLC) test fixture, 2023.

[28] Deutsches Institut für Normung, DIN EN ISO 14125, fibre-reinforced plastic composites - determination of flexural properties, 2011.

[29] J. Wang, K.D. Potter, K. Hazra, Wisnom, Experimental fabrication and characterization of out-of-plane fiber waviness in continuous fiber-reinforced composites, J. Compos. Mater. 46 (17) (2012) 2041–2053, http://dx.doi.org/10.1177/0021998311429877.

[30] M. Nartey, T. Zhang, B. Gong, J. Wang, S. Peng, H. Wang, H.-X. Peng, Understanding the impact of fibre wrinkle architectures on composite laminates through tailored gaps and overlaps, Compos. Part B: Eng. 196 (2020) 108097, http://dx.doi.org/10.1016/j.compositesb.2020.108097.

[31] J. Drummer, F. Tafesh, B. Fiedler, Effect of fiber misalignment and environmental temperature on the compressive behavior of fiber composites, Polymers 15 (13) (2023) 2833, http://dx.doi.org/10.3390/polym15132833.

[32] T.W. Riddle, J.W. Nelson, D.S. Cairns, Effects of defects in composite wind turbine blades – part 3: A framework for treating defects as uncertainty variables for blade analysis, Wind. Energy Sci. 3 (1) (2018) 107–120, http://dx.doi.org/10.5194/wes-3-107-2018.

[33] J.W. Nelson, T.W. Riddle, D.S. Cairns, Effects of defects in composite wind turbine blades – part 1: Characterization and mechanical testing, Wind. Energy Sci. 2 (2) (2017) 641–652, http://dx.doi.org/10.5194/wes-2-641-2017.

[34] I. Solodov, Y. Bernhardt, L. Littner, M. Kreutzbruck, Ultrasonic anisotropy in composites: Effects and applications, J. Compos. Sci. 6 (3) (2022) 93, http://dx.doi.org/10.3390/jcs6030093.

[35] I.A. Viktorov, Rayleigh and lamb waves: Physical theory and applications, Softcover reprint of the hardcover 1st edition 1967, Ultrasonic technology, Springer Science+Business Media, New York, 2013, URL: https://permalink.obvsg.at/AC16322516.

[36] C. Wu, Y. Gu, L. Luo, P. Xu, S. Wang, M. Li, Z. Zhang, Influences of in-plane and out-of-plane fiber waviness on mechanical properties of carbon fiber composite laminate, J. Reinf. Plast. Compos. 37 (13) (2018) 877–891, http://dx.doi.org/10.1177/0731684418765981.

[37] J. Mandell, D. Samborsky, L. Wang, Effects of fiber waviness on composites for wind turbine blades, Mater. Sci. Eng. (2003) URL: https://www.scopus.com/inward/record.uri?eid=2-s2.0-0842311503&partnerID=40&md5=c6f3f52c4d6b6c62fdbfc480bc95150c.

[38] P. Kulkarni, K.D. Mali, S. Singh, An overview of the formation of fibre waviness and its effect on the mechanical performance of fibre reinforced polymer composites, Compos. Part A: Appl. Sci. Manuf. 137 (2020) 106013, http://dx.doi.org/10.1016/j.compositesa.2020.106013.

[39] J.J. Bender, S.R. Hallett, E. Lindgaard, Investigation of the effect of wrinkle features on wind turbine blade sub-structure strength, Compos. Struct. 218 (2019) 39–49, http://dx.doi.org/10.1016/j.compstruct.2019.03.026.

[40] S. Mukhopadhyay, M.I. Jones, S.R. Hallett, Tensile failure of laminates containing an embedded wrinkle; numerical and experimental study, Compos. Part A: Appl. Sci. Manuf. 77 (2015) 219–228, http://dx.doi.org/10.1016/j.compositesa.2015.07.007.

[41] L.D. Bloom, J. Wang, K. Potter, Damage progression and defect sensitivity: An experimental study of representative wrinkles in tension, Compos. Part B: Eng. 45 (1) (2013) 449–458, http://dx.doi.org/10.1016/j.compositesb.2012.05.021.

[42] W. Woigk, S.R. Hallett, M.I. Jones, M. Kuhtz, A. Hornig, M. Gude, Experimental investigation of the effect of defects in automated fibre placement produced composite laminates, Compos. Struct. 201 (2018) 1004–1017, http://dx.doi.org/10.1016/j.compstruct.2018.06.078.

[43] B. Wang, N. Uda, K. Ono, H. Nagai, Effect of micro in-plane fiber waviness on compressive properties of unidirectional fabric composites, J. Compos. Mater. 52 (15) (2018) 2065–2074, http://dx.doi.org/10.1177/0021998317740197.

[44] S.S. Nimbal, M.M. Banker, A. Roopa, B. Varughese, R. Sundaram, Effect of gap induced waviness on compressive strength of laminated composites, Mater. Today: Proc. 4 (8) (2017) 8355–8369, http://dx.doi.org/10.1016/j.matpr.2017.07.179.

[45] Y. Yuan, X. Yao, K. Niu, B. Liu, Q. Wuyun, Compressive failure of fiber reinforced polymer composites by imperfection, Compos. Part A: Appl. Sci. Manuf. 118 (2019) 106–116, http://dx.doi.org/10.1016/j.compositesa.2018.12.017.

[46] S.L. Lemanski, M. Sutcliffe, Compressive failure of finite size unidirectional composite laminates with a region of fibre waviness, Compos. Part A: Appl. Sci. Manuf. 43 (3) (2012) 435–444, http://dx.doi.org/10.1016/j.compositesa.2011.11.007.

[47] R.F. Elhajjar, S.S. Shams, Compression testing of continuous fiber reinforced polymer composites with out-of-plane fiber waviness and circular notches, Polym. Test. 35 (2014) 45–55, http://dx.doi.org/10.1016/j.polymertesting.2014.02.004.

[48] D.O. Adams, S.J. Bell, Compression strength reductions in composite laminates due to multiple-layer waviness, Compos. Sci. Technol. 53 (2) (1995) 207–212, http://dx.doi.org/10.1016/0266-3538(95)00020-8.

[49] D. O'Hare Adams, M.W. Hyer, Effects of layer waviness on the compression strength of thermoplastic composite laminates, J. Reinf. Plast. Compos. 12 (4) (1993) 414–429, http://dx.doi.org/10.1177/073168449301200404.

[50] B.D. Allison, J.L. Evans, Effect of fiber waviness on the bending behavior of S-glass/epoxy composites, Mater. Des. (1980- 2015) 36 (2012) 316–322, http://dx.doi.org/10.1016/j.matdes.2011.11.012.

[51] ABAQUS/Explicit, VUMAT for Fabric Reinforced Composites, Providence, RI, USA, Dassault Systèmes Simulia Corp, 2008.

[52] T. Wagner, S. Heimbs, F. Franke, U. Burger, P. Middendorf, Experimental and numerical assessment of aerospace grade composites based on high-velocity impact experiments, Compos. Struct. 204 (2018) 142–152, http://dx.doi.org/10.1016/j.compstruct.2018.07.019.

[53] M.J. Donough, B.G. Prusty, M.J. Van Donselaar, E.V. Morozov, H. Wang, P.J. Hazell, A.W. Philips, N.A. St John, In-plane and oblique edge-on impact on thick glass-fibre/epoxy composite laminates, Int. J. Impact Eng. 171 (2023) 104373, http://dx.doi.org/10.1016/j.ijimpeng.2022.104373.

[54] B.F. Sørensen, S. Goutianos, L.P. Mikkelsen, S. Fæster, Fatigue damage growth and fatigue life of unidirectional composites, Compos. Sci. Technol. 211 (2021) 108656, http://dx.doi.org/10.1016/j.compscitech.2021.108656.

[55] S. Hörrmann, A. Adumitroaie, M. Schagerl, The effect of ply folds as manufacturing defect on the fatigue life of CFRP materials, Frat. Ed IntegritÀ Strutt. 10 (38) (2016) 76–81, http://dx.doi.org/10.3221/IGF-ESIS.38.10.

[56] H.G. Mendonça, L.P. Mikkelsen, B. Zhang, G. Allegri, S.R. Hallett, Fatigue delaminations in composites for wind turbine blades with artificial wrinkle defects, Int. J. Fatigue 175 (2023) 107822, http://dx.doi.org/10.1016/j.ijfatigue.2023.107822.